2010-01-01

Design And Simulation Of A Position Sensitive Device With Gaussian Response

Debra Erin Medina
University of Texas at El Paso, dmedina@utep.edu

DESIGN AND SIMULATION OF A POSITION SENSITIVE DEVICE WITH GAUSSIAN RESPONSE

DEBRA ERIN MEDINA

Department of Electrical Engineering

APPROVED:

_____
John Moya, Ph.D., Chair

_____
John McClure, Ph.D.

_____
Gregory Lush, Ph.D.

_____
Eric MacDonald, Ph.D.

_____
Pablo Arenaz, Ph.D.
Dean of Graduate School

DESIGN AND SIMULATION OF A POSITION SENSITIVE DEVICE WITH GAUSSIAN RESPONSE

by

DEBRA ERIN MEDINA, BSEE

THESIS

Presented to the Faculty of the Graduate School of

The University of Texas at El Paso

in partial fulfillment

of the Requirements

for the Degree of

MASTER OF SCIENCE

Department of Electrical Engineering

THE UNIVERSITY OF TEXAS AT EL PASO

May 2006

ABSTRACT

This thesis describes a new approach for designing position sensitive devices (PSD). Rather than trying to obtain a linear response to a light source this design takes advantage of the nonlinearities present in existing devices. Specifically it uses a p-n junction to obtain a Gaussian-shaped response curve to light. Using such response curves, two-dimensional position detection of an object can be accomplished with three detectors. The sensitivity of this PSD may be independent of the size of the light source and the device may not need calibration.

TABLE OF CONTENTS

Page

LIST OF TABLES

TABLE OF FIGURES

Chapter 1

INTRODUCTION

1.1 Position Sensitive Devices

A position sensitive device (PSD) is an optical sensor which is capable of estimating the centroid, or "center of mass", of a light spot hitting its surface. PSDs produce a current flow proportional to the intensity and position of light incident on the surface of the device. This information may then used to determine the actual position of the light spot.

There are currently two general types of PSDs which are capable of measuring lateral displacement in two dimensions. The first group, and most commonly used PSD, is referred to as lateral effect photodiodes [MAKY2003]. These devices consist of a single large-area photodiode with four contacts positioned at opposite edges of the device. The photon-generated current is divided between the contacts in proportion to the resistance of the current paths between the illuminated region and the contacts. Therefore the current flow through the contacts is directly related to the distance between the contact and light spot.

The second group of PSDs is referred to as quad detectors. These devices consist of four photodiodes symmetrically positioned around the center of the device. Position information is determined by the strength of the signal received by each of the quadrants. The electrical contribution of each signal is then used to determine

the relative position of light with respect to the center of the device. The structure as well as the detailed operation of these devices is described in Chapter 2.

1.2 Applications

Position sensitive devices are used for a variety of commercial applications, for instance, in consumer products PSDs are used for tasks such as precision position sensing and auto-focusing in photographic and video cameras [FRAD2004]. PSDs are typically favored over other imaging devices such as charge-coupled devices (CCDs) in high volume applications where signal processing, high speed, robustness, and low cost are of importance.

These devices also have industrial applications, including the for measurement of small displacements. As such, they are sometimes used for machine tool alignment [KOMA1996] and optical lateral, rotational or angular position sensing [CHOW1998]. Further, PSDs may take precise measurements of device height in applications like printed-circuit board inspection, liquid and solids-level control, laser torch height control, etc. They may also be used for thickness and precision displacement measurements. These latter types of measurements can be useful in detecting the presence or absence of an object such as a medicine bottle cap.

1.3 Purpose

Existing PSDs have a linear response characteristic near the center of the device but exhibit non-linear properties toward the outer edges. Typically research efforts are focused on improving the linearity of the response of PSDs [CONN1971][MORI1991], so the current produced when light is incident on the surface is directly proportional to the distance between the light spot and the electrode throughout the entire surface of the device. However there is a potential benefit for the use of the nonlinear properties inherent in PSDs. Moya presents an algorithm that makes it possible to do position detection with a sensor that has a Gaussian response rather than a linear response [MOYA2005]. This thesis describes the benefits of taking advantage of these nonlinearities as well as a proposed structure for a PSD.

1.4 Overview of Thesis

Chapter 2 provides background information and an overview of previous work on PSDs, including detailed information about their operation and the structure of commonly used PSDs. It also compares their performance and describes their advantages as well as their disadvantages.

Chapter3 offers a new approach to designing PSDs. The structure of the device is proposed and necessary equations derived. It also contains the simulation that shows the device performance using Microsoft Excel.

Chapter 4 provides the simulation results and describes some additional work that can be performed to obtain more accurate results concerning the actual performance of the proposed device. Concluding remarks are also presented.

Chapter 2

BACKGROUND

There are two general types of PSDs, lateral effect photodiodes and quad detectors. Lateral effect photodiodes can determine the absolute distance of movement while quad detectors can only reveal the direction once the spot is displaced more than its radius from a center point [YANG2002].

The performance of a PSD is based on certain criteria:

(1) Position resolution, which is the minimum detectable displacement of a light spot on the detector's surface. High resolution indicates a small minimum detectable displacement.

(2) Speed of its performance, the amount of time it takes to detect the position of a light spot

(3) Difficulty of fabrication, the more complex the PSD structure the more costly it is to fabricate.

2.1 Lateral Effect Photodiodes

The measurement span of the lateral-effect photodiode is determined by the size of its active area. Its signals are a direct measure of the position of the light spot center from the edges of the detector.

The side view of a typical one-dimensional lateral effect photodiode is shown in Figure 2.1. This one-dimensional form has two electrodes (labeled A and B) on the upper p-type layer to provide electrical contacts. It also contains an additional electrode (labeled C) on the N^+ layer to provide a biasing voltage.

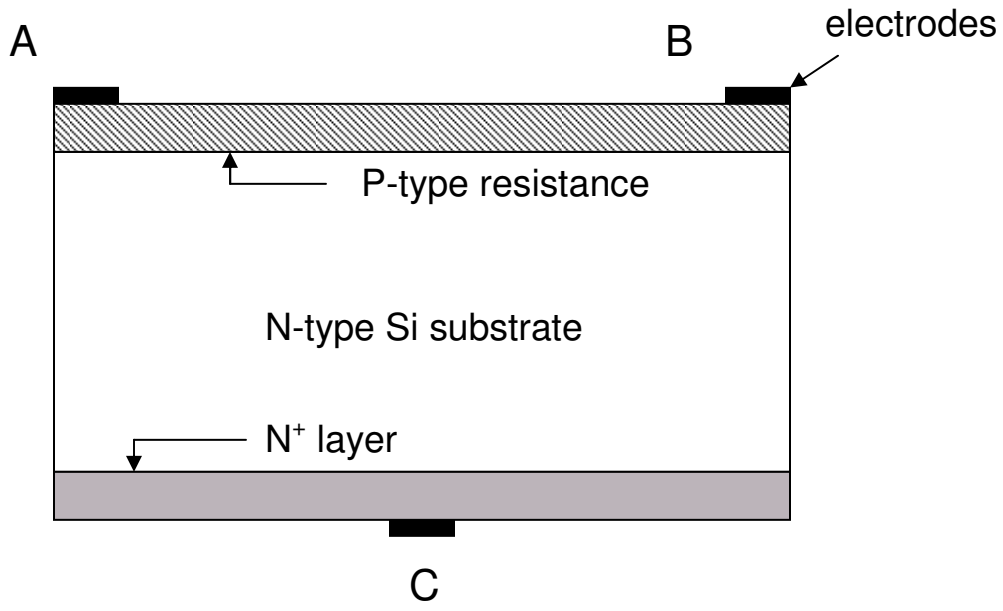

Figure 2.1: Side view of one-dimensional lateral-effect photodiode.

The operation of this device is based on the lateral photoelectric effect; when a semiconductor junction is non-uniformly illuminated by radiant energy (light), a lateral photovoltage is established. The magnitude and polarity of the lateral photovoltage varies as the light spot moves between the contacts.

Position information is determined by the difference-to-sum ratio of the current at electrodes A and B. This is given by equation (2.1) [CHOW1998].

$$I = \frac{Ix_A - Ix_B}{Ix_A + Ix_B} \tag{2.1}$$

Various geometries and materials have been used to construct lateral effect photodiodes. The most common material used is silicon and the geometries most often studied for two dimensional versions include tetralateral, duolateral dual-axis, pincushion, and clover [WANG1989].

2.1.1 Tetralateral PSD Form

The tetra-lateral version is one of the most commonly studied geometries for a two-dimensional detector [WANG1989], and several papers have been written describing its operation [CONN1971], [WOLT1975], [SHAE1998]. It is illustrated in Figure 2.2 and consists of four electrodes, one on each side of a square sensing area. The difference-to-sum ratio of currents on opposite sides of the device are used to find the Cartesian two-dimensional coordinates of a light spot. The X-coordinate of the incident light is the difference between currents x1 and x2 and the Y-coordinate is the difference between currents y1 and y2. This device may be operated in any spatial orientation; the X and Y direction assignments are arbitrary.

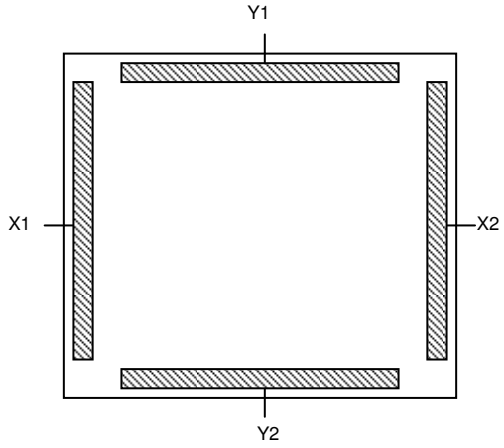

Figure 2.2: Tetra-lateral PSD geometry. Shaded areas indicate electrodes.

This device is linear near its center but has a large distortion near the edges of its active area because neighboring contacts interfere with each other. This can cause a position error of about 12% [CHOW1998].

2.1.2 Dual-Axis Duolateral Form

The dual-axis duolateral form consists of an n-type silicon substrate with two resistive layers. The first resistive layer is p-type with ohmic contacts on two opposite sides of the device while the other is n-type with contacts orthogonal to those of the first layer. This device is illustrated in Figure 2.3.

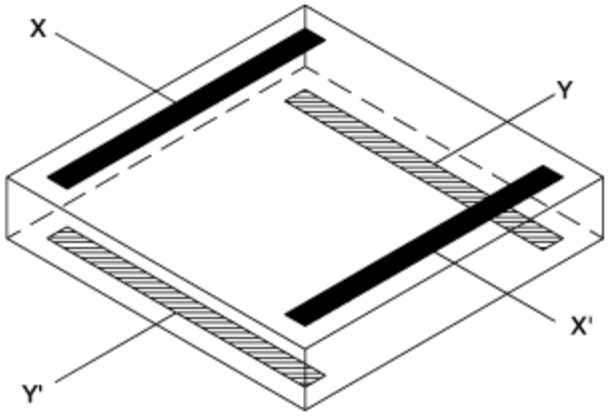

Figure 2.3: Dual-lateral PSD structure.

The resolution of this device is twice that of the tetralateral PSD because the generated photocurrent is only divided into two parts rather than four. Thus, better linearity can be achieved. However, this device produces a large dark current [MORI1991], so it is often reverse-biased in operation. This device also has some other disadvantages when compared to the tetralateral PSD: it has both a slower response and is more expensive to fabricate because it requires contacts to be placed on both sides of the device.

2.1.3 Pincushion Form

The pincushion version attempts to combine the best aspects of both the dual-axis duolateral and the tetralateral forms. It has contacts on only one side of the p-

n junction and minimizes interference between the x and y outputs through careful selection of the boundary shape of the junction surface, the sheet resistance, and electrode shapes. As illustrated in Figure 2.4, the boundaries of this device are curved rather than straight. The active sensing area is comprised of a rectangle whose sides are tangent to the innermost points on the curved boundaries. The electrical contacts are located at the four corners of the device.

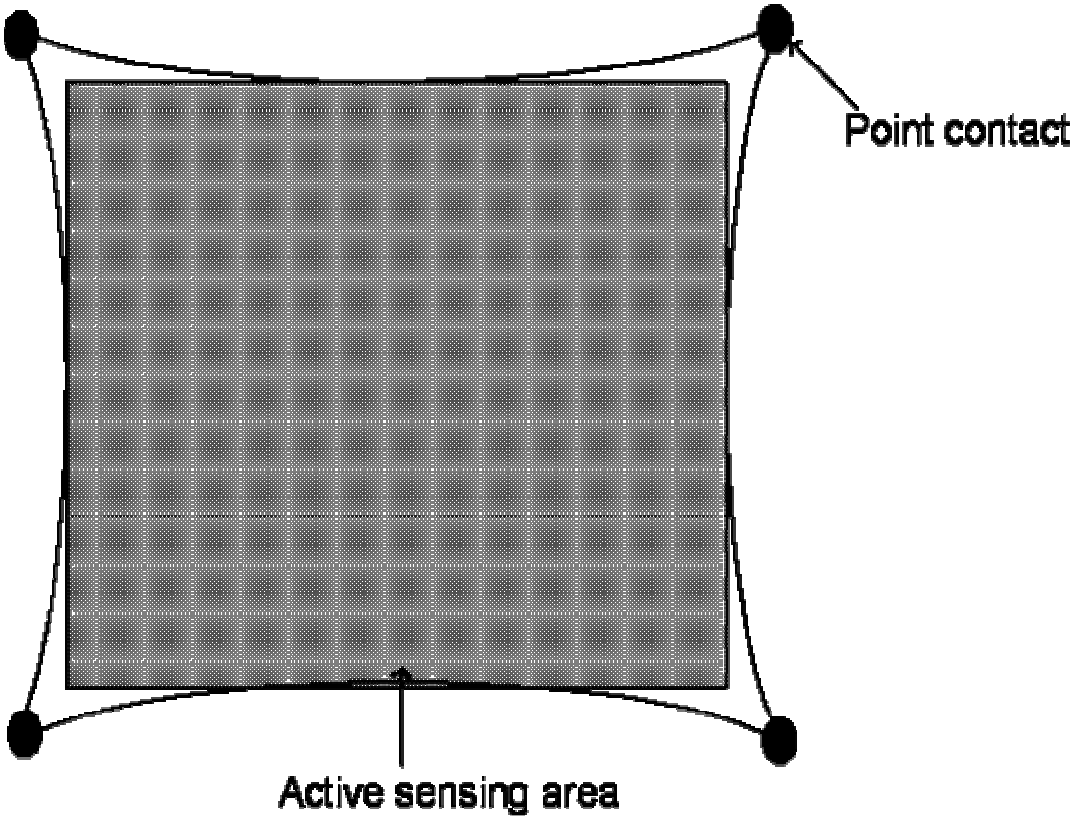

Figure 2.4: Pincusion PSD geometry.

The pincushion detector is linear over a much broader range of its active surface than the tetralateral PSDs [WANG1989]. However, the ratio of sensitive area to the total area is small because of its curved boundaries [DOKE1987].

2.1.4 Clover Form

As illustrated in Figure 2.5, the clover version contains eight protruding point contacts and four short contacts at its corners. The sensitivity of this detector is about five times that of the pincushion form while its maximum distortion is lower [WANG1989]. Further its resolution is roughly twice that of the tetralateral and about equal to that of the duolateral form [CONN1971]. However, this structure produces large leakage currents.

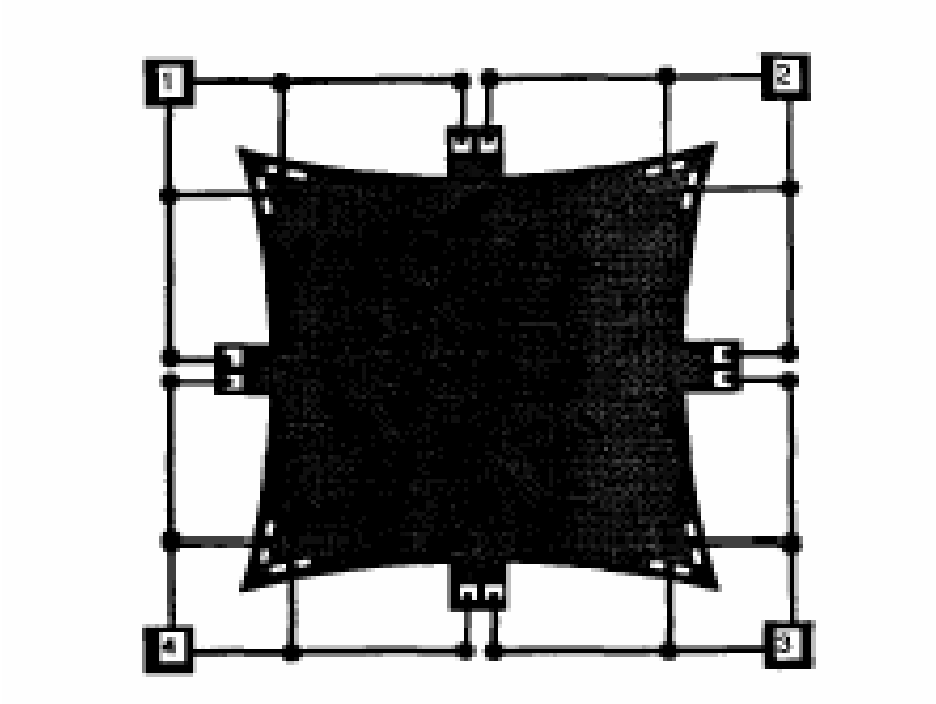

Figure 2.5: Structure of clover PSD.

2.1.5 Other Methods

Other techniques have been used to increase the resolution of a position sensitive device and to improve the linearity of its response. These include using

MOSFETS to change a conventional dual-axis simultaneous sensing method into a single but alternate-axis sensing one. The latter results in linearity equivalent to that of a one-dimensional PSD [MORI1991].

Reverse biasing the PSD may also result in higher resolution, because of the increase in thickness of the depletion layer between the p and n layers. This effectively reduces the current through the device to almost zero, preventing surface recombination [CONN1971].

Other approaches include using different materials as a substitute for Silicon. These materials include Gallium Arsenide and Gold/Beta Silicon Carbide.

2.1.6 Summary

Different geometries such as the dual-axis duolateral, pincushion, and clover have improved detection linearity over the tetralateral PSD. The dual-axis duolateral and pincushion have low sensitivity and are nonlinear near the extreme edges of the device. The clover has an approximate linear response, however it has a complex shape and a large non-sensitive surface area [COWI1997]. Due to low active area resistance this latter device is also sensitive to biasing voltage [MURO1990], which can cause a DC offset current to flow. However, reverse-biasing the device can make it insensitive to background illumination and produce a higher resolution [CONN1971]. A comparison of the performance of three geometries, the tetralateral, pincushion, and clover, is given in Table 2-1.

Table 2-1: Comparison of measured linearity of various PSDs within 4 X4 mm² [YOUN1992].

Device	Percentage of area with distortion less than:					
	3%	5%	7%	9%	11%	20%
Tetralateral	10	15	21	25	30	52
Pincushion	20	36	52	80	100	100
clover	30	46	64	88	100	100

2.1.7 Disadvantages

In general lateral effect photodiodes can only be used to measure the absolute displacement of a light spot. Figure 2.6 illustrates that because these devices have an approximately linear response, a light spot initially in position A moving the same distance and in the same direction as a light spot initially in position B will produce equivalent difference-to-sum currents. Therefore, it is necessary to calibrate the device in order to know the initial position of the light source.

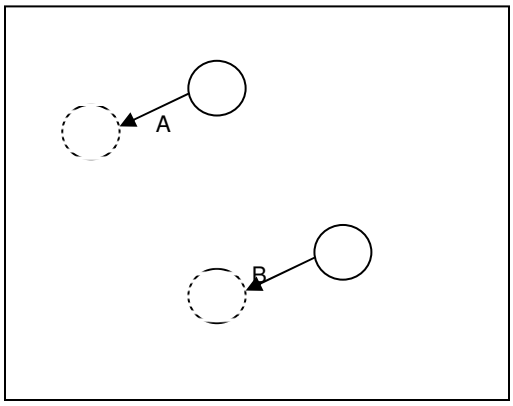

Figure 2.6: Light spots A and B at different initial positions moving the same distance and direction will produce equal outputs.

In addition, none of the devices described above provide a linear response for the entire sensing area. Therefore, they give inaccurate position information when the light centroid approaches the edges of the device. Finally, the sensitivity of these devices is dependent on spot size, as spot size is increased the sensitivity decreases [CHOW1998].

2.2 Quad detector

2.2.1 Structure

Another PSD structure is the quad detector depicted in Figure 2.7. It consists of four double junction photodiodes separated by vias. This device measures the displacement of a light spot with respect to the center of the quad cell. In order to operate, this device needs to be calibrated and the light spot must initially be at the center of the quad cell.

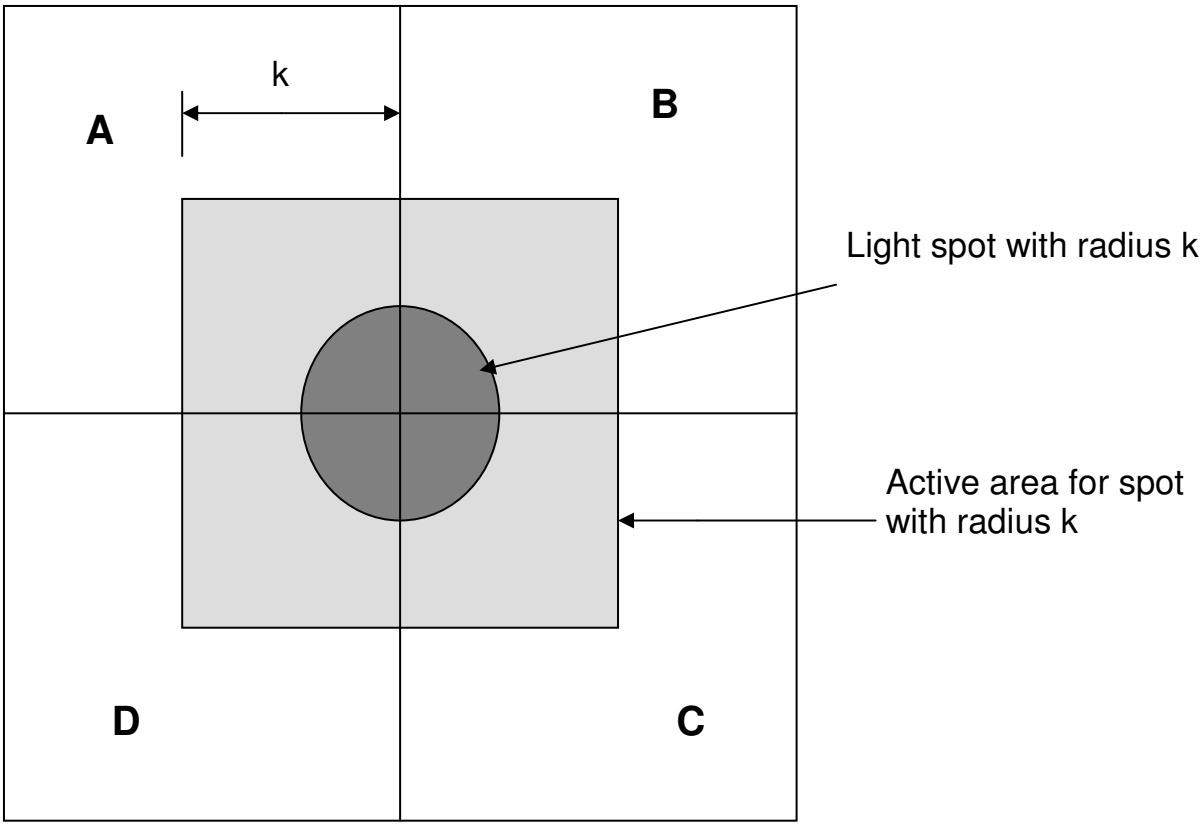

Figure 2.7: Quad cell structure with light spot of radius k at the center.

2.2.2 Operation

The centroid position of the light spot can be determined by performing relatively simple mathematical calculations on its output signals. The x-coordinate position is given by equation (2.2) and the y-coordinate position is given by equation (2.3) [DELI2001]. The current at each quadrant is represented in the equation by the variable, *I,* and the subscripts refer to a particular quadrant illustrated in Figure 2.7.

$$x = \frac{(I_B + I_C) - (I_A + I_D)}{I_A + I_B + I_C + I_D} \tag{2.2}$$

$$y = \frac{(I_A + I_B) - (I_C + I_D)}{I_A + I_B + I_C + I_D} \tag{2.3}$$

2.2.3 Disadvantages

The response of the quad cell PSD depends on the spot intensity and spot diameter. The maximum distance the spot can move from the center of the cell, and still provide position information, is called the spatial dynamic range and is approximately equal to the spot diameter. Once the light spot moves beyond this distance its position can no longer be precisely detected.

This device is also only linear for displacements near the center [DELI2004]. The transfer characteristics for a uniform circular spot are non-linear because the movement of the spot is not proportional to the percentage of the area which shifts between adjacent quadrants [MAKY1996]. Due to their highly nonlinear characteristics, quad detectors are thus most commonly used for tracking and centering devices rather than position sensors.

Chapter 3

METHOD OF IMPROVEMENT AND THEIR MODELING

A potential solution to the problems encountered with the various existing PSDs would be to take advantage of the nonlinearities present in the operation of these devices, instead of attempting to eliminate. Based on the algorithm presented by [MOYA2005] one can perform position detection using a sensor with a Gaussian-shaped response curve to light. In one dimension two such sensors are needed to identify the position of an object and for two-dimensional detection three curves are needed. This is illustrated in Figure 3.1. Applying their algorithm would allow the structure of the PSD device to be simplified. Futhermore, performance may be less affected by the size of the light spot and the device would not need calibration to determine the initial position of the object.

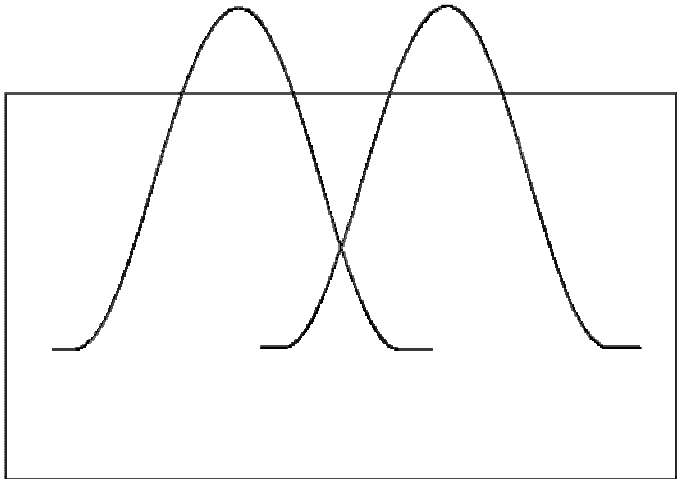

(a)

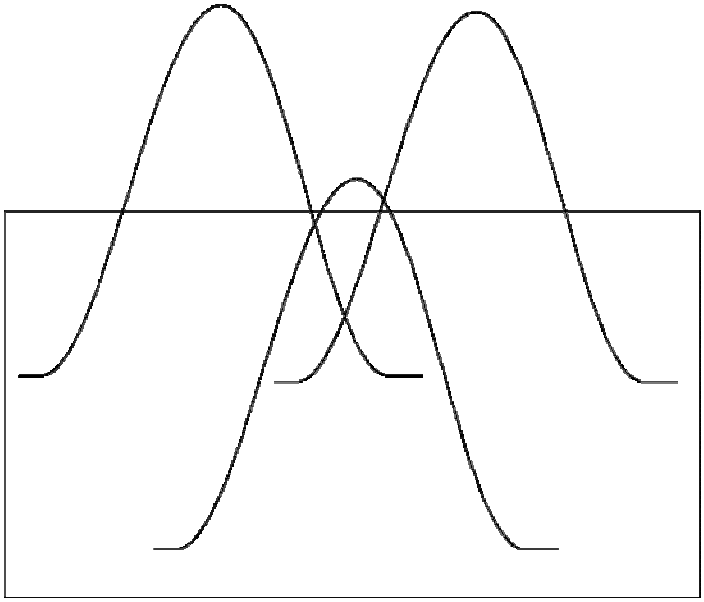

(b)

Figure 3.1: Overlapping Gaussian response curves used for (a) one-dimensional position detection and (b) two-dimensional position detection.

3.1 Structure

A structure with a Gaussian response can potentially be created with a p-n junction. This device would consist of an n-type substrate with a shallow p-type implant and metal contact as illustrated in Figure 3.2 and Figure 3.3.

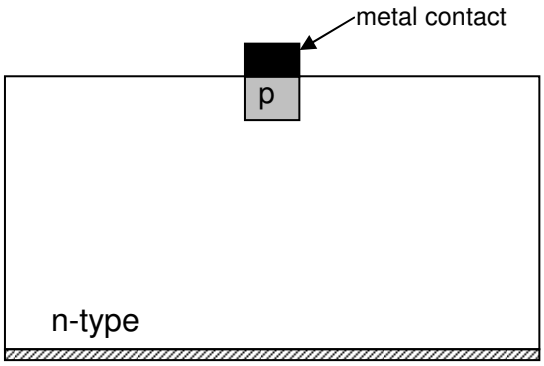

Figure 3.2: Side view of device with pn junction.

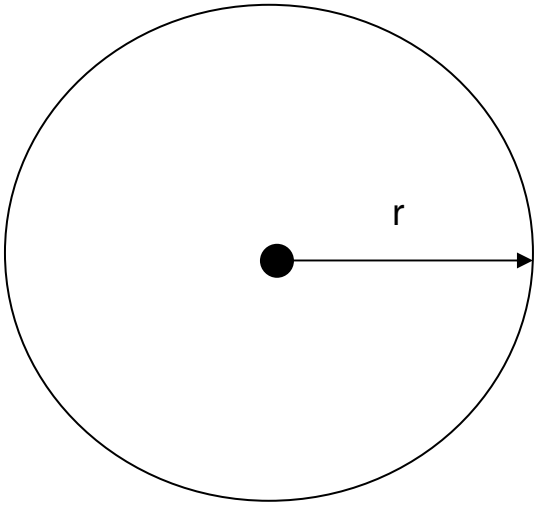

Figure 3.3: Top view of device.

3.2 Verification

In order to verify that the proposed structure in Figure 3.2 produces a Gaussian-shaped response curve to a light spot the device was simulated using

Microsoft Excel. The appropriate equations were derived and applied. A spreadsheet was then set-up to perform the calculations.

3.2.1 Computation

To simulate the device in Microsoft Excel a two-dimensional equation which described the behavior of excess holes in a semiconductor device was derived. The final equation varied with radial distance from the center of the device as well as depth within the device.

The net increase in the number of holes per unit time in a differential volume is given by Equation (3.1), which represents a three-dimensional continuity equation for using cylindrical coordinates. It is used to determine the concentration of excess carriers at each point in the device. The first term on the right-hand side of the equation is the increase in number of holes per unit time due to particle flux, the second term is the increase in number of holes due to the generation rate (g_p), and the final term is the decrease in number of holes due to recombination [NEAM1997].

$$\frac{\partial \Delta p}{\partial t} d\phi dr dz = -\nabla \bullet F_p{}^{+} d\phi dr dz + g_p d\phi dr dz - \frac{\Delta p}{\tau_p} d\phi dr dz \qquad (3.1)$$

The net increase in hole concentration can be found by dividing (3.1) by the differential volume, $d\phi drdz$. The resulting equation is the continuity equation for holes and is given by

$$\frac{\partial \Delta p}{\partial t} = -\nabla \bullet F_p^{+} + g_p - \frac{\Delta p}{\tau_p} \tag{3.2}$$

The total current density in a semiconductor is given by

$$J = en\mu_n E + ep\mu_p E + eD_n \nabla n - eD_p \nabla p \tag{3.3}$$

The four components of this latter equation are electron drift and diffusion currents and hole drift and diffusion currents. The sum of these four current mechanisms provides the total current density. The terms in the equation are defined below:

J= current density (A/cm^2)

e = electronic charge (magnitude)= 1.6 X 10^{-19} Coulombs

n,p= electron and hole concentration (cm^{-3})

μ_n,μ_p=electron and hole mobility (cm^2/V-sec)

E = Electric field (V/cm)

D_n,D_p=minority carrier electron and minority carrier hole diffusion coefficient (cm^2/sec)

$\nabla n, \nabla p =$ electron density gradient and hole density gradient

For the purposes of simulation, only the current generated by the movement of holes was taken into consideration. Thus, (3.3) was reduced to

$$J_p = ep\mu_p E - eD_p \nabla p \tag{3.4}$$

By dividing Equation (3.4) by an electron charge (e), the equation for particle flux can be obtained. This equation is given by

$$F_p^{+} = \mu_p pE - D_p \nabla p \tag{3.5}$$

Thus, the particle flux depends on the hole mobility (μ_p), the density of holes (p), the electric field (E), the diffusion coefficient D_p, and the hole gradient.

Substituting Equation (3.5) into the continuity Equation (3.2) yields

$$\frac{\partial \Delta p}{\partial t} = -\nabla \bullet \left[\mu_p pE - D_p \nabla p \right] + g_p - \frac{\Delta p}{\tau_p} \tag{3.6}$$

The term outside the brackets may be distributed to obtain

$$\frac{\partial \Delta p}{\partial t} = -\mu_p \nabla \bullet pE + D_p \left[\nabla \bullet \nabla p \right] + g_p - \frac{\Delta p}{\tau_p} \tag{3.7}$$

Noting that

$$\nabla\bullet(pE) = p\nabla\bullet E + E\nabla\bullet p \tag{3.8}$$

the first term in equation (3.7) may be expanded as shown in (3.9) and the second term as shown in (3.10).

$$-\mu_p \nabla\bullet pE = -\mu_p \left[p\left(\frac{1}{r}\frac{\partial}{\partial r}(rE_r) + \frac{1}{r}\frac{\partial E_\phi}{\partial \phi} + \frac{\partial E_z}{\partial z}\right) + E\left(\frac{1}{r}\frac{\partial}{\partial r}(rp_r) + \frac{1}{r}\frac{\partial p_\phi}{\partial \phi} + \frac{\partial p_z}{\partial z}\right)\right] \tag{3.9}$$

$$D_p\left[\nabla\bullet\nabla p\right] = D_p\left[\frac{1}{r}\frac{\partial}{\partial r}\left(r\frac{\partial \Delta p}{\partial r}\right) + \frac{1}{r^2}\frac{\partial^2 \Delta p}{\partial \phi^2} + \frac{\partial^2 \Delta p}{\partial z^2}\right] \tag{3.10}$$

In order to simplify the minority carrier diffusion equation the following assumptions are made [PIER1996]:

1. The system under analysis is two-dimensional, dependent only on radius, r, and depth, z.
2. The analysis is resticted to minority carriers
3. The electric field in the semiconductor is approximately zero, which allows its effects to be negligible.
4. The equilibrium minority carrier concentrations are not a function of position.

5. Low-level injection conditions exist ($\Delta p << n_0$)

6 Indirect thermal recombination-generation is the dominant thermal R-G mechanism

7. The only process taking place within the system is photogeneration.

The above assumptions allow equation (3.7) to be reduced to two-dimensions. It also allows all terms that include the electric field, E, to be eliminated. The resulting differential equation is given by

$$D_p\left[\left(\frac{1}{r}\right)\left(\frac{\partial \Delta p}{\partial r}\right)+\frac{\partial^2 \Delta p}{\partial r^2}+\frac{\partial^2 \Delta p}{\partial z^2}\right]+g(z)-\frac{\Delta p}{\tau_r}=\frac{\partial \Delta p}{\partial \Delta t} \qquad (3.11)$$

In (3.11) g(z) is the generation rate of carriers. It is assumed that g(z) = 0 if the semiconductor is not subject to illumination. To obtain a steady-state solution it is assumed that the change in concentration of holes does not vary with time. Therefore, $\frac{\partial \Delta p}{\partial t} \to 0$.

For use in Microsoft Excel, Equation (3.11) must be converted into a discrete equation rather than a continuous differential equation. This allows the differential equation to be solved at discrete points in the device. The conversion is completed by first approximating the derivative via the following definition:

$$\lim_{\Delta x \to 0} \frac{\Delta y}{\Delta x} = \frac{dy}{dx} \qquad (3.12)$$

To estimate the derivative in a region, Equation (3.13) can be used. The lower case □ is used as a substitute for the "□" in equation (3.12) because □ is used in the following equations to mean "change" while □ will be used to represent "difference".

$$\frac{\partial \Delta p}{\partial t} \approx \frac{\delta \Delta p}{\delta t} \tag{3.13}$$

To estimate the first derivative, (3.14) was substituted into (3.11) similarly, in terms that contained the second derivative, (3.15) was substituted into those terms.

$$\frac{d\Delta p}{dt} \approx \frac{\Delta p_{i+1} - \Delta p_i}{\delta t} \tag{3.14}$$

$$\frac{d^2 \Delta p}{dx^2} \approx \frac{\Delta p_{i,j+1} - 2\Delta p_{i,j} + \Delta p_{i,j-1}}{\delta x^2} \tag{3.15}$$

With the above substitutions, the following minority carrier diffusion equation is obtained:

$$0 = D_p \left[\frac{1}{r} \left(\frac{\Delta p_{i+1,j} - \Delta p_{i,j}}{\delta r} \right) + \frac{\Delta p_{i+1,j} - 2\Delta p_{i,j} + \Delta p_{i-1,j}}{\delta r^2} + \frac{\Delta p_{i,j+1} - 2\Delta p_{i,j} + \Delta p_{i,j-1}}{\delta z^2} \right] + g(z) - \frac{\Delta p_{i,j}}{\tau} \tag{3.16}$$

The terms were rearranged to solve for □ $p_{i,j}$. The resulting equation that was used in Excel is

$$\Delta p_{i,j} = \frac{\frac{g(z)}{D_p} + \Delta p_{i+1,j}\left[\frac{1}{r\delta r} + \frac{1}{\delta r^2}\right] + \frac{\Delta p_{i-1,j}}{\delta r^2} + \frac{\Delta p_{i,j+1}}{\delta z^2} + \frac{\Delta p_{i,j-1}}{\delta z^2}}{\frac{1}{r\delta r} + \frac{2}{\delta r^2} + \frac{2}{\delta z^2} + \frac{1}{D_p \tau_r}} \tag{3.17}$$

3.2.2 Simulation

For purposes of simulation, a cylindrical device with a radius of 0.1 cm and a depth of 5mm is assumed. The p-type junction was placed at the center of the device.

A spreadsheet was then setup in Excel in which each cell represented the carrier concentration at a discrete point in the device. The spreadsheet consisted of a 100 X 100 array of cells in which the columns represented the radial distance from the contact and the rows represented depth in the device.

As can be seen in (3.17), the result in each cell depends on its surrounding cells. The *i* subscript in the equation refers to a particular column while *j* specifies a particular row. The cell layout with reference to the subscripts is illustrated in Figure 3.4.

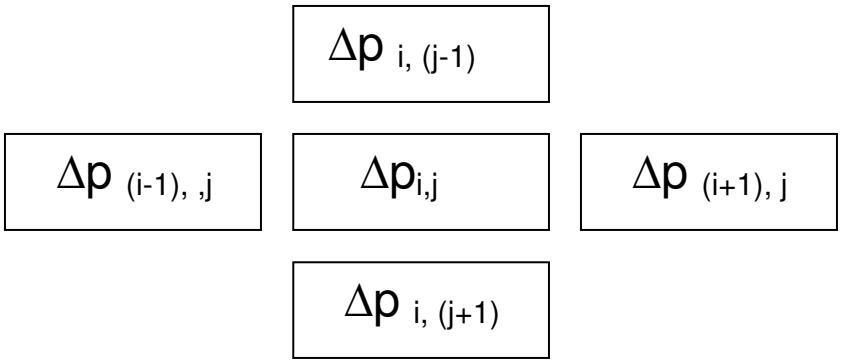

Figure 3.4: Cell layout in Excel spreadsheet.

Thus, when the value in a cell changes, this causes a change in the surrounding cells. In order to find a stabilization point, a maximum iterative change must be defined. Therefore, within the Excel simulations, calculations in the spreadsheet continue within an iteration until the maximum change in the values, for all cells, from one iteration to another iteration, are less than $1*10^{-9}$.

At the left boundary of the spreadsheet the slope was set to zero. This was done by referencing the cell to the right ($\Delta p_{(i+1),j}$) rather than the one to the left for the entire left column. This allows the device to be symmetrical about the far left column. For the remaining boundaries, top, right, and bottom, the values in the cells beneath, to the left, and above, respectively, were copied into the boundary cells. For instance, the values in row two were copied into the cells that comprise the uppermost row of the array.

The generation rate for carriers, g(z), varied with depth and was calculated using

$$g(z) = i\alpha \exp(-\alpha z) \tag{3.18}$$

where *i,* is the light intensity ($10cm^{-2}$) and α is the absorption coefficient ($1000\ cm^{-1}$).

During simulation, generation of carriers took place in only one column at a time, emulating the effects of a light source at different radial distances from the central point of the device. The active column in Excel was indicated by a value of one in a row at the top of the simulation array where all other entries were zeroes. The Microsoft Excel spreadsheet set-up is illustrated in Figure 3.5.

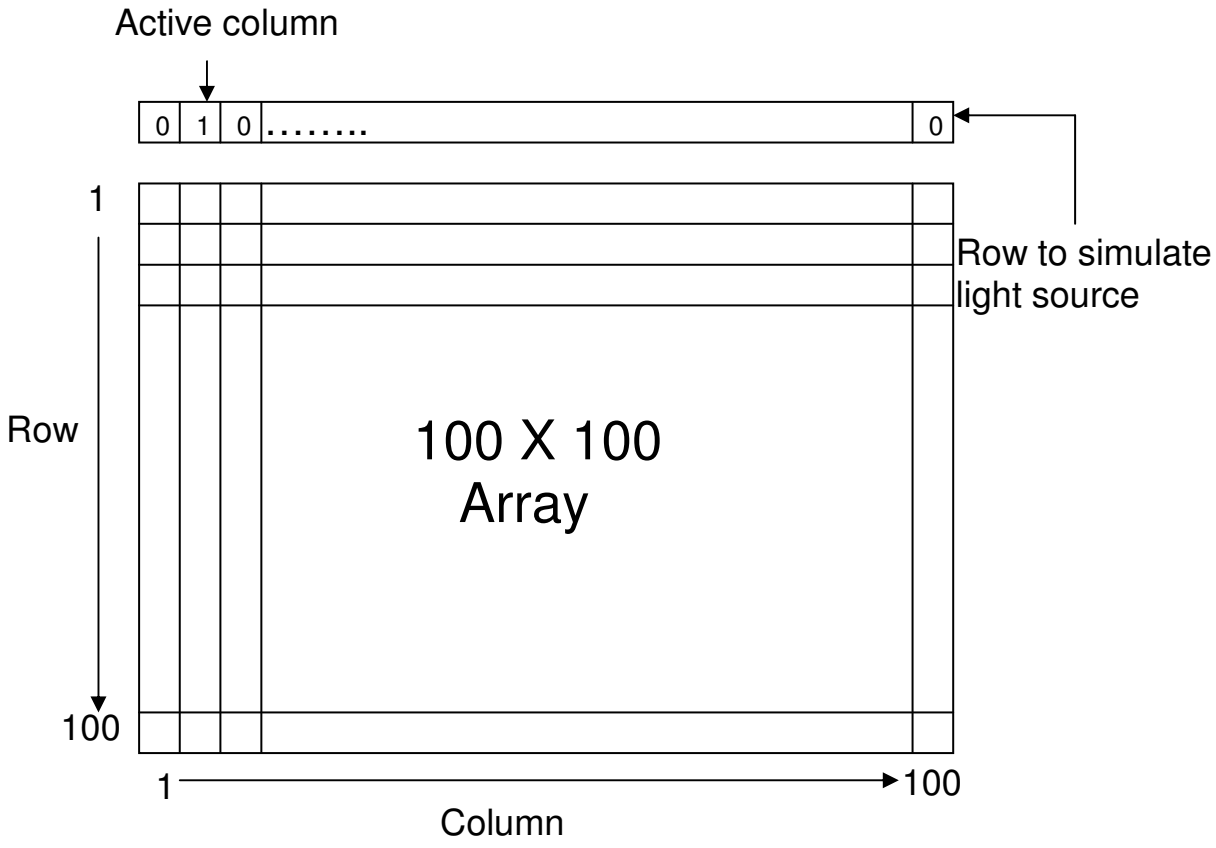

Figure 3.5: Solar cell spread sheet set-up in Excel.

This additional control on generation can be incorporated into Equation (3.17) using a term A via

$$\Delta p_{i,j} = \frac{\left(\frac{g(z)}{D_p}\right)A + \Delta p_{i+1,j}\left[\frac{1}{r\delta r} + \frac{1}{\delta r^2}\right] + \frac{\Delta p_{i-1,j}}{\delta r^2} + \frac{\Delta p_{i,j+1}}{\delta z^2} + \frac{\Delta p_{i,j-1}}{\delta z^2}}{\frac{1}{r\delta r} + \frac{2}{\delta r^2} + \frac{2}{\delta z^2} + \frac{1}{D_p \tau_r}} \tag{3.19}$$

When the cell above a column is zero (i.e. A = 0) there is no generation of carriers taking place in that column.

Simulations were done initially by activating each of the 100 columns one by one. However, it was determined that sufficiently accurate results could by obtained by activating every fifth column.

After the simulation was run with one column active the resulting current density was calculated using

$$J = -qD_p\left[\frac{\Delta p}{\Delta r} + \frac{\Delta p}{\Delta z}\right] \tag{3.20}$$

The current was then calculated by applying

$$I = \oint_s \vec{J} \bullet d\vec{s} \tag{3.21}$$

A screenshot of the Excel spreadsheet is shown in Figure 3.6. All the constants used in the simulation are on the left side of the spreadsheet. The column labeled "Generation" shows how the generation rate of carriers varies with the depth of the device. The top row simulates the light source. In this screenshot, the second column is generating carries because there is a "1" above the corresponding column, all other columns contain zeros.

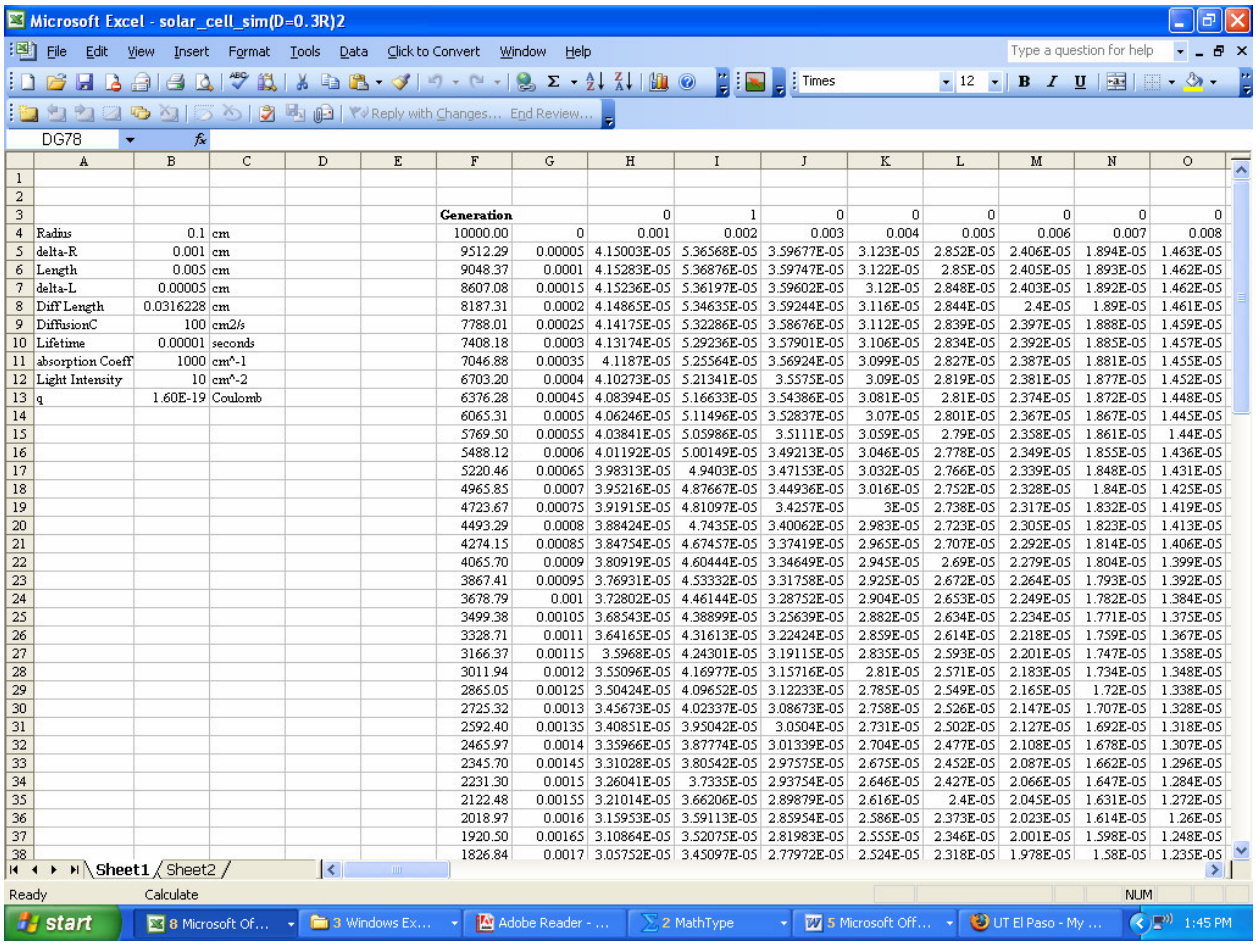

	A	B	C	D	E	F	G	H	I	J	K	L	M	N	O
1															
2															
3						Generation		0	1	0	0	0	0	0	0
4	Radius	0.1	cm			10000.00	0	0.001	0.002	0.003	0.004	0.005	0.006	0.007	0.008
5	delta-R	0.001	cm			9512.29	0.00005	4.15003E-05	5.36568E-05	3.59677E-05	3.123E-05	2.852E-05	2.406E-05	1.894E-05	1.463E-05
6	Length	0.005	cm			9048.37	0.0001	4.15283E-05	5.36876E-05	3.59747E-05	3.122E-05	2.85E-05	2.405E-05	1.893E-05	1.462E-05
7	delta-L	0.00005	cm			8607.08	0.00015	4.15236E-05	5.36197E-05	3.59602E-05	3.12E-05	2.848E-05	2.403E-05	1.892E-05	1.462E-05
8	Diff Length	0.0316228	cm			8187.31	0.0002	4.14865E-05	5.34635E-05	3.59244E-05	3.116E-05	2.844E-05	2.4E-05	1.89E-05	1.461E-05
9	DiffusionC	100	cm2/s			7788.01	0.00025	4.14175E-05	5.32286E-05	3.58676E-05	3.112E-05	2.839E-05	2.397E-05	1.888E-05	1.459E-05
10	Lifetime	0.00001	seconds			7408.18	0.0003	4.13174E-05	5.29236E-05	3.57901E-05	3.106E-05	2.834E-05	2.392E-05	1.885E-05	1.457E-05
11	absorption Coeff	1000	cm^-1			7046.88	0.00035	4.1187E-05	5.25564E-05	3.56924E-05	3.099E-05	2.827E-05	2.387E-05	1.881E-05	1.455E-05
12	Light Intensity	10	cm^-2			6703.20	0.0004	4.10273E-05	5.21341E-05	3.5575E-05	3.09E-05	2.819E-05	2.381E-05	1.877E-05	1.452E-05
13	q	1.60E-19	Coulomb			6376.28	0.00045	4.08394E-05	5.16633E-05	3.54386E-05	3.081E-05	2.81E-05	2.374E-05	1.872E-05	1.448E-05
14						6065.31	0.0005	4.06246E-05	5.11496E-05	3.52837E-05	3.07E-05	2.801E-05	2.367E-05	1.867E-05	1.445E-05
15						5769.50	0.00055	4.03841E-05	5.05986E-05	3.5111E-05	3.059E-05	2.79E-05	2.358E-05	1.861E-05	1.44E-05
16						5488.12	0.0006	4.01192E-05	5.00149E-05	3.49213E-05	3.046E-05	2.778E-05	2.349E-05	1.855E-05	1.436E-05
17						5220.46	0.00065	3.98313E-05	4.9403E-05	3.47153E-05	3.032E-05	2.766E-05	2.339E-05	1.848E-05	1.431E-05
18						4965.85	0.0007	3.95216E-05	4.87667E-05	3.44936E-05	3.016E-05	2.752E-05	2.328E-05	1.84E-05	1.425E-05
19						4723.67	0.00075	3.91915E-05	4.81097E-05	3.4257E-05	3E-05	2.738E-05	2.317E-05	1.832E-05	1.419E-05
20						4493.29	0.0008	3.88424E-05	4.7435E-05	3.40062E-05	2.983E-05	2.723E-05	2.305E-05	1.823E-05	1.413E-05
21						4274.15	0.00085	3.84754E-05	4.67457E-05	3.37419E-05	2.965E-05	2.707E-05	2.292E-05	1.814E-05	1.406E-05
22						4065.70	0.0009	3.80919E-05	4.60444E-05	3.34649E-05	2.945E-05	2.69E-05	2.279E-05	1.804E-05	1.399E-05
23						3867.41	0.00095	3.76931E-05	4.53332E-05	3.31758E-05	2.925E-05	2.672E-05	2.264E-05	1.793E-05	1.392E-05
24						3678.79	0.001	3.72802E-05	4.46144E-05	3.28752E-05	2.904E-05	2.653E-05	2.249E-05	1.782E-05	1.384E-05
25						3499.38	0.00105	3.68543E-05	4.38899E-05	3.25639E-05	2.882E-05	2.634E-05	2.234E-05	1.771E-05	1.375E-05
26						3328.71	0.0011	3.64165E-05	4.31613E-05	3.22424E-05	2.859E-05	2.614E-05	2.218E-05	1.759E-05	1.367E-05
27						3166.37	0.00115	3.5968E-05	4.24301E-05	3.19115E-05	2.835E-05	2.593E-05	2.201E-05	1.747E-05	1.358E-05
28						3011.94	0.0012	3.55096E-05	4.16977E-05	3.15716E-05	2.81E-05	2.571E-05	2.183E-05	1.734E-05	1.348E-05
29						2865.05	0.00125	3.50424E-05	4.09652E-05	3.12233E-05	2.785E-05	2.549E-05	2.165E-05	1.72E-05	1.338E-05
30						2725.32	0.0013	3.45673E-05	4.02337E-05	3.08673E-05	2.758E-05	2.526E-05	2.147E-05	1.707E-05	1.328E-05
31						2592.40	0.00135	3.40851E-05	3.95042E-05	3.0504E-05	2.731E-05	2.502E-05	2.127E-05	1.692E-05	1.318E-05
32						2465.97	0.0014	3.35966E-05	3.87774E-05	3.01339E-05	2.704E-05	2.477E-05	2.108E-05	1.678E-05	1.307E-05
33						2345.70	0.00145	3.31028E-05	3.80542E-05	2.97575E-05	2.675E-05	2.452E-05	2.087E-05	1.662E-05	1.296E-05
34						2231.30	0.0015	3.26041E-05	3.7335E-05	2.93754E-05	2.646E-05	2.427E-05	2.066E-05	1.647E-05	1.284E-05
35						2122.48	0.00155	3.21014E-05	3.66206E-05	2.89879E-05	2.616E-05	2.4E-05	2.045E-05	1.631E-05	1.272E-05
36						2018.97	0.0016	3.15953E-05	3.59113E-05	2.85954E-05	2.586E-05	2.373E-05	2.023E-05	1.614E-05	1.26E-05
37						1920.50	0.00165	3.10864E-05	3.52075E-05	2.81983E-05	2.555E-05	2.346E-05	2.001E-05	1.598E-05	1.248E-05
38						1826.84	0.0017	3.05752E-05	3.45097E-05	2.77972E-05	2.524E-05	2.318E-05	1.978E-05	1.58E-05	1.235E-05

Figure 3.6: Screenshot of Microsoft Excel worksheet.

This simulation procedure was performed for varying values of the diffusion length. In the spreadsheet the diffusion length was calculated by applying equation

$$Diffustion\_Length = \sqrt{D_p \tau_p} \tag{3.22}$$

All values, except the diffusion coefficient, D_p, were held constant from simulation to simulation. The simulation was performed for the following three values of diffusion length in relation to the radius of the device.

(1) *Diffusion_length = (1/3)*r*

(2) *Diffusion_length = r*

(3) *Diffusion_length = 3*r*

The value for the hole lifetime, τ_p, remained at 10 microseconds for all three simulations.

Chapter 4

RESULTS AND CONCLUSIONS

4.1 Simulation Results

Simulation results for the three simulations, *D=1/3r, D=r, and D=3r*, are given in Table 4-1 and plotted in Figure 4.1.

Table 4-1: Current produced for various radial distances for three simulations.

Radius	D=0.3R	D=R	D=3R
0.005	0.223901	0.22716	0.22529
0.01	0.201452	0.212312	0.221985
0.0153	0.175711	0.193206	0.211564
0.02	0.158731	0.178175	0.194498
0.025	0.141801	0.160933	0.178411
0.03	0.126017	0.145881	0.161601
0.035	0.11251	0.128635	0.147915
0.04	0.103054	0.117	0.135706
0.045	0.096543	0.107895	0.125064
0.05	0.092768	0.100167	0.115132
0.055	0.088342	0.095122	0.107501
0.06	0.085995	0.090991	0.100459
0.065	0.083071	0.087742	0.094509
0.07	0.082784	0.085076	0.090722
0.075	0.082038	0.08351	0.087778
0.08	0.081609	0.081609	0.084644
0.085	0.080927	0.080927	0.082376
0.09	0.080486	0.080486	0.080486
0.095	0.079891	0.079891	0.079891
0.1	0.079301	0.079301	0.079301

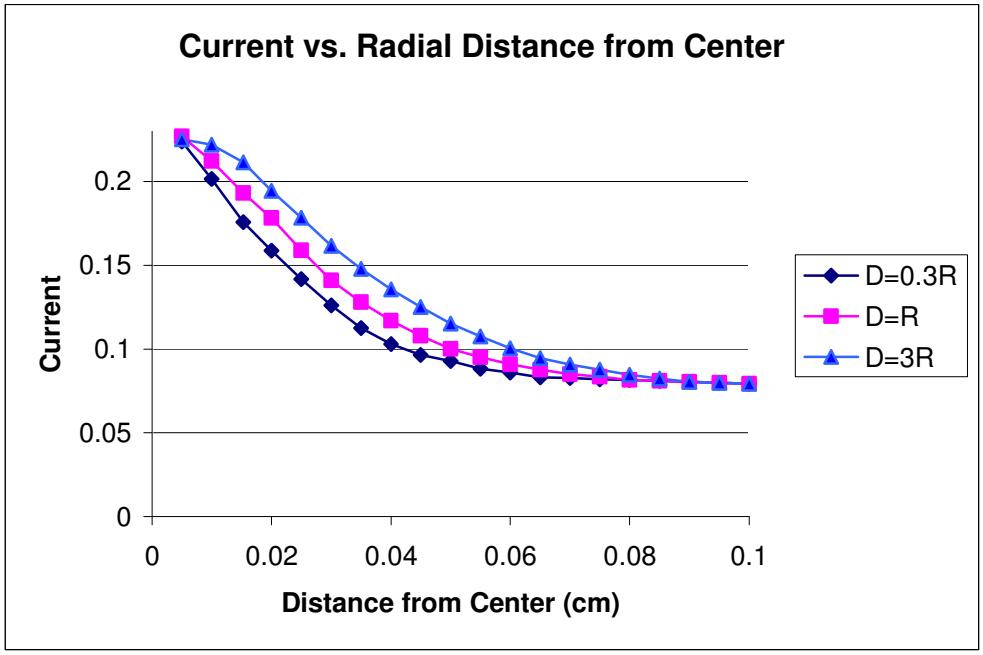

Figure 4.1: Plot of data points given in table 2.

The data points obtained for the first simulation, in which D =1/3r, were fitted to a Guassian function. The general equation for a Gaussian function is given by

$$Y = A * \exp(-X^2 / X_0^2) \qquad (4.1)$$

Where the values A and X_0 are constants that were changed to fit the data points. The value 'A' was approximated by the y-intercept of the simulation data points. The value for 'X_0' was found by trial and error. The resulting fitted equation is given by

$$Y = 0.1544\exp(-X^2/0.027566^2) + 0.0712 \qquad (4.2)$$

As illustrated in Figure 4.2 the response of the device decreases as the distance from the p-n junction increases and the simulation data points fit to the Gaussian equation (4.2).

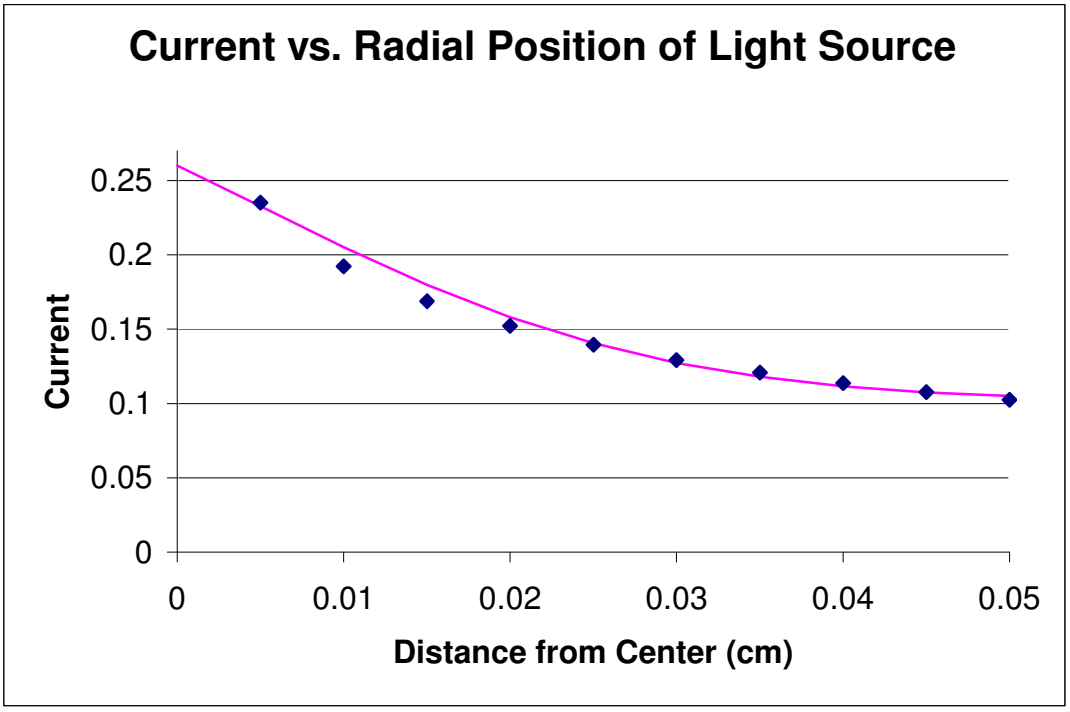

Figure 4.2: The resulting data points fit to a Gaussian curve.

These results verify that the proposed structure produces a Gaussian-shaped response to a light stimulus. In order to acheive overlapping Gaussian curves, as is needed for two-dimensional poisition detection, more p-type implants must be added to the device.

4.2 Other Simulations

In addition to the discrete simulation described in the previous chapter the minority carrier diffusion equation given in the (3.12) was also solved using a different approach. Granville Sewell simulated the continuous equation using a partial differential equation solver called PDE2D.

4.2.1 PDE2D

The software package solves general partial differential equations (PDEs) in two or three dimensions. For a two-dimensional problem a Galerkin finite element method, with isoparametric triangular elements of up to 4th degree is used. Adaptive refinement and grading of the triangular mesh are available for 2D problems [SEWE2005]. In order to use the software to solve a two-dimensional equation the user must answer a series of questions about the region, partial differential equations and boundary conditions, and select solution method and graphical output options. The interactive driver automatically writes a FORTRAN program, based on the user's answers, which is then compiled and linked to the PDE2D library routines it calls.

4.2.2 Simulation results

The simulation was run using the same parameters for device size, generation rate, and boundary conditions as those used in the simulation described in chapter 3. The results obtained by Sewell are given in Table 4-2.

Table 4-2: Results from PDE2D simulation.

Radius	Current
0.005	0.235182
0.01	0.19235
0.015	0.168807
0.02	0.152235
0.025	0.139513
0.03	0.129293
0.035	0.120856
0.04	0.113768
0.045	0.107742
0.05	0.102581

4.2.3 Comparison

When the simulation values obtained by Sewell were plotted on the same axis as those found using Microsoft Excel the results were found to be similar but not identical as illustrated in Figure 4.3. A possible explanation for the variation in results between those found using Microsoft Excel and those found by using the software package PDE2D is that the former solved the equation at discrete points while the latter method solved the continuous equation.

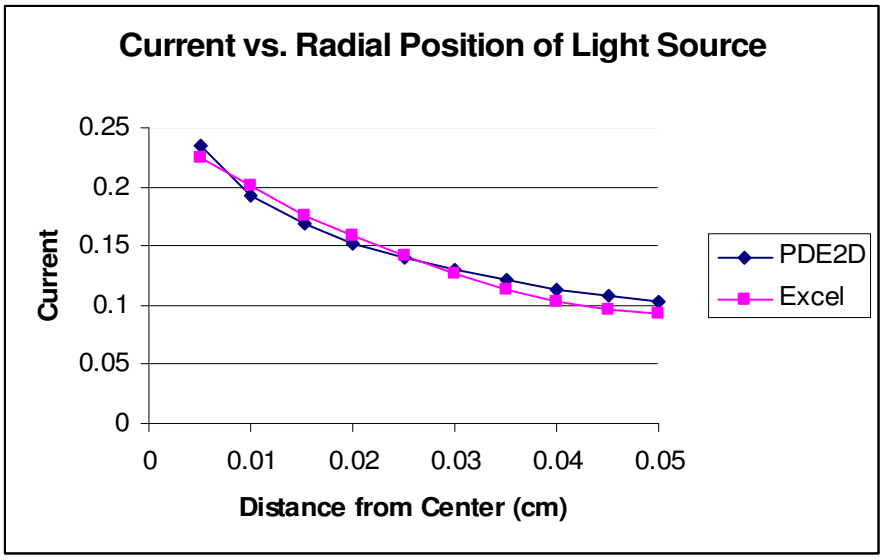

Figure 4.3: Plot of simulation results obtained from Microsoft Excel and PDE2D on same axis.

4.3 Conclusions and Future Work

The proposed device offers several advantages when compared to existing PSDs. The structure is very simple. It consists of an n-type substrate with a p-type implant and metal contact. This will allow the device to be relatively inexpensive to fabricate. Second, the device does not need to be initially calibrated because the response is Gaussian and the output would depend on the initial position as well as the final position. Finally, the operation of the device may be independent of spot size and light intensity.

The results obtained from the simulation verify that the proposed structure produces a Gaussian-shaped response to a light stimulus. In order to achieve overlapping Gaussian curves, as is needed for two-dimensional position detection, more p-type implants must be added to the device.

The device proposed has a simple structure which would make it relatively inexpensive to fabricate. This gives it another advantage over existing PSDs that are generally complicated.

In order to obtain more conclusive evidence concerning the performance of the device it must be fabricated and tested using a light source. The results provided in this thesis were based only on theoretical calculations.

Once this device is constructed more definitive operational results can be determined, such as its resolution, operational speed, etc. Then it can be compared to existing PSDs to determine if it in fact produces a more accurate result.

REFERENCES

[CHOW1998] M. F. Chowdhury, "CMOS 1D and 2D N-well Tetra-lateral Position Sensitive Detectors," *IEEE Transactions Electron Devices*, pp 606-609, 1998.

[CONN1971] William P. Connors, "Lateral Photodetector Operating in the Fully Reverse-Biased Mode," IEEE *Transactions on Electron Devices*, pp 591-596, 1971.

[COWI1997] R.L. Cowin and D. L. Watson, "Surface Charge Flow in Two-Dimensional Position Sensitive Silcon Detectors," *Nuclear Instruments and Methods in Physics Research,* A399, pp 365-381, 1997.

[DELI2001] D.W. de Lima Monteiro, G. Vdovin and M. Loktev, "IC-Compatible optical sensor for Adaptive Optics," *Microwave and optoelectronics Conference*. IMOC 2001. Proceedings of the 2001 SBMO/IEEE MTT-S International, vol 1, pp 513-516, 2001.

[DELI2004] D. W. de Lima Monteiro, G. Vdovin, P.M. Sarro, "High-speed wavefront sensor compatible with standard CMOS technology," *Sensors and Actuators A(Physical),* vol. A109, no.3, pp 220-230, 2004.

[DOKE1987] Ladayoshi Doke, “A New Two-Dimensional Position Sensitive Detector with Good Linear Response,” *Nuclear Instruments and Methods in Physics Research*, A261, pp 605-609, 1987.

[FRAD2004] Fraden, Jacob. "Handbook of Modern Sensors", 3rd edition New York: Springer-Verlag New York, Inc., 2004.

[KOMA1996] Komatsu, M, Ohkawa, K, Tsuchida, N, Imai, K. “Hole position and inclination sensor with 2 dimensional PSD, and its application to automatic shaft inserting”, *Multisensor Fusion and Integration for Intelligent Systems, 1996. IEEE International Conference on 8-11 Dec.* 1996, pp. 78-85.

[MAKY1996] Anssi Makynen, Juha Kostamovaara, and Risto Myllyla, “Positioning Resolution of the Position-Sensitive Detectors in High Background Illumination,” *IEEE Transactions on Instrumentation and Measurement*, vol 45, no. 1, pp 324-326, 1996.

[MAKY2003] Anssi Makynen, Tarmo Tuotsalainen, Timo Rahkonen, and Juha Kostamovaara, “CMOS-compatible position-sensitive devices (PSDs) based on photodetector arrays,” *Sensors and Actuators A: Physical*, vol 105, issue 3, pp 261-270, 2003.

[MORI1991] Morikawa and Kawamura, “A Small Distortion Two-Dimensional Position-Sensitive Detector(PSD) with On-Chip

MOSFET Switches," *IEEE Transactions on Electron Devices*, vol 34, pp723-726, 1991.

[MOYA2005] John Moya and David Saenz

[MURO1990] H. Muro and P. J. French, "An Integrated Position Sensor Using JFETs as a Buffer for PSD Output Signal", *Sensors and Actuators*, pp 522-544, 1990.

[NEAM1997] Donald Neaman. "Semiconductor Physics and Devices", Second edition The McGraw-Hill Companies, Inc. 1997.

[PIER1996] Robert F. Pierret, Semiconductor Device Fundamentals, Addison-Wesley Publishing Company, Inc. 1996.

[SEWE2005] Granville Sewell, The Numerical Solution of Ordinary and Partial Differential Equations, Second Edition, John Wiley & Sons, 2005.

www.pde2d.com

[SHAE1998] Shaefer and D. Williams, "Accuracy of Position Detection Using a Position-Sensitive Detector," *IEEE Transactions on Instrumentation and Measurement*, vol 47, pp 914-919,1998.

[WANG1989] Wang and Busch-Vishniac, "The Linearity and Sensitivity of Lateral Effect Position Sensitive Devices-An Improved Geometry," *IEEE Transactions on Electron Devices*, vol. 36, pp2475-2480, 1989.

[WOLT1975] H.J. Woltring, "Single and dual-axis lateral photodetectors of rectangular shape," *IEEE Transactions on Electron Devices*, vol. 22 pp 581-586, 1975.

[YANG2002] Tsung-Yi Yang, James Gourlay, and Andrew C. Walker, "Adaptive Alignment Packaging for 2-D Arrays of Free-Space Optical-Interconnected Optoelectronic Systems," *IEEE Transactions on Advanced Packaging*, vol. 25, no. 1, pp 54-64, 2002.

[YOUN1992] Kim Youngmin, "Fabrication and Characterization of a clover Type Position Sensitive Detector," *Instrumentation and measurement technology conference proceedings*, pp 404-408, May 12-14, 1992.

CURRICULUM VITA

Debra Medina was born in El Paso, TX. She is the second daughter of Charles and Elia Medina. She graduated from Eastwood High School in El Paso, TX in the spring of 1999. After graduation she pursued a bachelor's degree in Electrical Engineering from the University of Texas at El Paso. She graduated in the spring of 2004. She continued her education at the University of Texas at El Paso and entered the Graduate School following the receipt of her Bachelor's Degree.

Permanent Address: 10848 Valle Grande
El Paso, TX 79935

This thesis was typed by the author.